Study of the roughness in a photoresist masked, isotropic, SF6-based ICP silicon etch

Larsen, Kristian Pontoppidan; Petersen, Dirch Hjorth; Hansen, Ole

Published in:
Journal of The Electrochemical Society

Link to article, DOI:
10.1149/1.2357723

Publication date:
2006

Document Version
Publisher's PDF, also known as Version of record

Journal of The Electrochemical Society, **153** (12) G1051-G1058 (2006)
0013-4651/2006/153(12)/G1051/8/$20.00 © The Electrochemical Society

Study of the Roughness in a Photoresist Masked, Isotropic, SF_6-Based ICP Silicon Etch

Kristian P. Larsen,[a] Dirch Hjorth Petersen,[a] and Ole Hansen[a,b,z]

[a]*MIC - Department of Micro and Nanotechnology, NanoDTU, and* [b]*Danish National Research Foundation's Center for Individual Nanoparticle Functionality (CINF), Technical University of Denmark, DK-2800 Kgs. Lyngby, Denmark*

In this paper we study the etching behavior and the resulting roughness in photoresist-masked isotropic silicon plasma etch performed in an inductively coupled plasma (ICP) etcher using SF_6. We report detailed observations of the resulting roughness for various etching parameters, covering: pressure from 2.5 to 70 mTorr, SF_6 flow rate from 50 to 300 sccm, platen power from 0 to 16 W, and ICP power from 1000 to 3000 W. Etch processes with a normalized roughness below 0.005 were found at low pressure, p = 10 mTorr, while larger normalized roughness, above 0.02, occurred at higher pressures, p = 40–70 mTorr. Here the normalized roughness is the ratio of the roughness amplitude to the etch depth. The rough etching processes showed characteristic high-aspect-ratio and crystal-orientation-dependent surface morphology. The temporal evolution of this roughness was studied, and observations suggest a gradual buildup of surface contamination (redeposits) originating from the photoresist mask. A model was used to analyze the etched profiles with respect the internal etching conditions. The almost isotropic etching profiles, obtained in both rough and smooth etching processes, are generally highly radical-dependent; however, the surface roughness itself can be reduced dramatically using an ion energy above a certain threshold value. The roughness causing mechanism is discussed.
 [DOI: 10.1149/1.2357723]

Manuscript submitted March 10, 2006; revised manuscript received June 1, 2006. Available electronically October 12, 2006.

Plasma etching and deep reactive ion etching (DRIE) in particular have become widely used for silicon micromachining. The plasma-based processes can provide highly anisotropic etching with excellent homogeneity and repeatability, a key to successful microfabrication. Also, in applications where an isotropic etch is desirable, plasma etching might be the process of choice. In most applications a smooth morphology of the etched surface is critically important; this is especially true for surfaces in optical and mechanical microsystems.[1] However, in some cases the etched surfaces show severe roughness, which can render the surface useless in these applications. Still rough surfaces may be used constructively if the roughness is well controlled. These surfaces can be used, e.g., for light absorbers,[2] highly effective area supports for catalysts, high-surface-energy surfaces,[3] or otherwise functional nanostructured surfaces. In any case, an understanding of the evolution of the roughness and the underlying reason for the resulting roughness is required.

The roughness created during the etching process is associated with more or less stochastic processes at the etched surface. The plasma-surface interactions involved are often very complex and not known in any detail. Several studies of the roughness resulting from silicon plasma etching have been performed on maskless substrates.[4-6] Here, the roughness is generally treated as intrinsic etch front instabilities due to redistribution of the F radicals, or induced directly by the ions[4] which assist the etch process. Other studies report on roughening observations ascribed to the presence of a passivation or micromasking layer originating from various contamination sources. Oxygen[7] or aluminum[8] contamination from the etch chamber is commonly observed. In the case of black silicon,[9] silicon micrograss is formed in a slightly overpassivated anisotropic etch due to a delicate balance between micromasking, ion flux and energy, and surface passivation. Photoresist masks are often claimed to cause roughness by redeposition on the surface being etched. However, to our knowledge, a detailed analysis of this mechanism has not been performed.

Here we studied the roughness formed in an almost isotropic, photoresist-masked silicon etch performed in a high-density inductively coupled plasma etcher (ICP) using pure SF_6. The resulting etch profiles are almost isotropic, since the pure SF_6 plasma lacks native passivation mechanisms at temperatures slightly above room temperature. The etch process is generally considered a chemical etch with the desorbtion of the etch product as the rate-limiting step, where an ion flux to the surface enhances the etch rate by assisting the desorbtion. The presence of the photoresist mask in the present study results in very high roughness amplitudes (several micrometers) and with a highly anisotropic, crystal-orientation-dependent morphology.

Crystallographic anisotropy has been observed for an SF_6-based etch at cryogenic temperatures, where the {111} planes are effectively passivated.[10,11] The crystallographically anisotropic roughness observed here also seems to be related to {111} planes of silicon; however, the appearances differ, which indicates that a different mechanism might be involved.

In this study we try to correlate the roughness distribution inside etched cavities to the complete shape of the etched cavity, taking into account also the influence of radical and ion flux to the surfaces as well as redeposits on the surfaces.

Experimental

Standard (100), 100 mm, 1–20 Ω cm n-type doped silicon wafers were masked with a 1.5 μm thick AZ5214E photoresist using standard UV lithography. The substrates were subsequently etched in an ICP etcher (Advanced Silicon Etch from STS) which has an aluminum chamber. The etching process was initiated with a 10 s surface cleaning etch step using 2800 W ICP power, 19 W platen power, 15 mTorr chamber pressure, and a flow rate of 260 sccm SF_6. This preconditioning step removes the native oxide on the silicon surfaces and etches 1.1 μm of the silicon, ensuring a smooth initial silicon surface for the next etch step. Without unloading the substrates they were then etched for 5 min using the specific continuous isotropic etching recipe based on pure SF_6 and no platen power (in most cases). An overview of the recipes used is given in Table I. For some selected recipes also the etch duration was varied, and etches with varying platen power (0–16 W) were carried out with recipe N and O. Finally, the resist mask was removed in acetone (it was experimentally shown that this acetone rinse did not influence the roughness measurement).

The mask design included circular holes and long trenches of window widths ranging from 7 to 180 μm. The global load (ratio of exposed to total wafer area) of the mask corresponds to ~10%.

The etched substrates were cleaved and cross sections of etched trenches were characterized using a scanning electron microscope (SEM). Cleaving was carried out along the (110) plane at the center axis of the substrates, which resulted in high-quality cross sections suitable for geometrical analysis. The roughness amplitude was also obtained from the SEM cross sections by manual measurement of the representative maximum valley-to-top distance at the bottom and

[z] E-mail: oh@mic.dtu.dk

Table I. Overview of the etching recipes used and resulting performance of the etch processes.

				Etch depth		Bottom roughness		Sidewall roughness	
Recipe ID	Pressure (mTorr)	Flow rate (sccm)	ICP power (W)	w_t = 7 μm (μm)	62 μm (μm)	Amplitude[a]	Type	Amplitude[a]	Type
A	2.5	50	1000	10.0	13.2	0.0058	II	0.0062	II
B	2.5	50	3000	11.3	14.7	0.013	III	0.019	III
C	10	50	1000	14.9	23.6	<0.0009	I	0.021	III
D	10	200	1000	16.4	25.6	0.0020	II	0.030	III
E	10	300	1000	16.3	24.7	0.0056	III	0.020	III
F	10	50	3000	15.8	24.5	0.0049	II–III	0.0084	II–III
G	10	200	3000	19.6	33.1	0.0008	I	0.015	III
H	11	300	3000	21.3	37.5	<0.0006	I	0.016	III
I	40	250	2000	29.9	56.3	0.018	IV	0.029	IV
J	70	50	1000	25.5	47.4	0.043	IV	0.033	IV
K	70	200	1000	28.2	52.1	0.019	IV	0.015	IV
L	70	300	1000	29.6	54.5	0.023	III–IV	0.027	III–IV
M	70	50	3000	32.1	59.6	0.051	IV	0.071	IV
N	70	200	3000	37.9	75.9	0.022	IV	0.038	IV
O[b]	70	200	3000	38.9	84.0	<0.0004	I	0.017	IV
P	70	300	3000	39.7	78.6	0.023	IV	0.028	IV

[a] Roughness amplitude in trenches with 62 μm mask width normalized to vertical (bottom) or horizontal (sidewall) etch depth.
[b] 16 W platen power was applied in this recipe.

at the sidewall regions. This was done since the topology of the etched profiles excluded the use of atomic force microscopy (AFM) characterization for the roughness. Unfortunately this results in less accurate quantification of the roughness. In order to analyze the etched profiles, the SEM cross sections were digitized and processed using Matlab.

Results

Roughness observations.— Table I and Fig. 1 summarize the roughness observations in the etch experiments. The results reported in Table I are values for trenches with a mask width of 62 μm obtained after an etch duration of 5 min. In order to make the roughness values comparable, the table shows roughness amplitudes that are normalized to the local etching depth, bottom etch depth, h_{bot}, or horizontal etch depth, h_{side}.

The appearance of the roughness has been categorized into four different types, as shown in Fig. 1.

Low bottom roughness (type I) is generally found for recipes at a pressure of $p \simeq 10$ mTorr. Recipe H with a high ICP power (3000 W) and a high flow rate (300 sccm) results in the lowest normalized bottom roughness of <0.0006, corresponding to <20 nm roughness amplitude in a 37.5 μm deep etch. The sidewall roughness has considerably larger amplitude and a typical wave-like geometry (type III).

At lower pressure, $p = 2.5$ mTorr, the etch result is somewhat rougher, typically with a flat granular roughness (type II), and a high ICP power (3000 W) increases that roughness. Here, the roughness amplitude is nearly the same at the bottom of the trench and at sidewalls.

Recipes using higher pressures, 40 or 70 mTorr, show a dramatic increase in the roughness. Here the roughness morphology is typically wave-like, type III, tending toward more faceted and straight-walled, type IV. The roughness has the largest amplitude for processes at a low flow rate (50 sccm). High ICP power tends to increase the roughness, and the largest roughness amplitude is found for recipe M (ICP power 3000 W, flow rate 50 sccm), with a normalized bottom roughness of 0.085, corresponding to an amplitude of 2.4 μm for a 28.4 μm deep etch. The etch profile of recipe M with a 7 μm mask window is shown in Fig. 2.

Collections of the etched profiles of typical rough ($p = 70$ mTorr) and smooth ($p = 10$ mTorr) etching processes are shown in Fig. 3. In the figure, the profiles are normalized to the width of the mask window of the trench, w_t. This normalization procedure is described further in the discussion.

Increasing the ion energy by applying a radio frequency platen power of 16 W (recipe O) (Fig. 4, right) has a dramatic impact on the roughness. The bottom surface becomes completely smooth and should be compared to the rough profile of recipe N (Fig. 4, left), which is obtained using essentially the same process parameters but without platen power. The roughness amplitude at varying platen power is shown in Fig. 5. Already at 4 W, the bottom roughness drops below 20 nm. The sidewall roughness also shows a reduction during this interval, but here the changes are more modest. At 2 W the bottom roughness is still present but significantly reduced. As seen in Fig. 5 the morphology now seems to be wavelike, type III. For higher platen powers the roughness amplitude drops below the measurement limit, and a clear trace from the mask shadow is formed, which widens a bit at increasing power. In the transition region between the smooth bottom to the shadowed areas, the amplitude rises quickly, again including type III roughness.

The overall etching profile of recipe O is comparable to the smooth profiles obtained at pressure $p = 10$ mTorr (Fig. 3, bottom), in contrast to the profile obtained using recipe N (Fig. 3, top).

The effects of the masking material and masking conditions have been investigated briefly. An etch at high pressure, $p = 70$ mTorr, which results in a high-amplitude roughness of type IV using resist masks, showed much lower roughness when an oxide mask was used. With the oxide mask the etched surfaces were generally smooth without any clear crystallographic anisotropy. When the platen power (16 W) was applied with the oxide mask, an increased but still low amplitude roughness was observed. Other studies have shown a strong impact on the resulting etch profiles when different mask materials were used.[12]

Maskless etch experiments were performed with recipes G and K. Here a 100 μm deep maskless etch of a structured surface produced low roughness, especially when recipe K was used. The appearance of the roughness was different from the roughness seen in the masked etch but comparable to roughness type I, as reported in Ref. 13.

Temporal evolution.— The temporal evolution of the roughness was investigated in the case of a very rough etch (recipe M). SEM images of the surfaces after an etch duration of 12, 25, 50, and 150 s

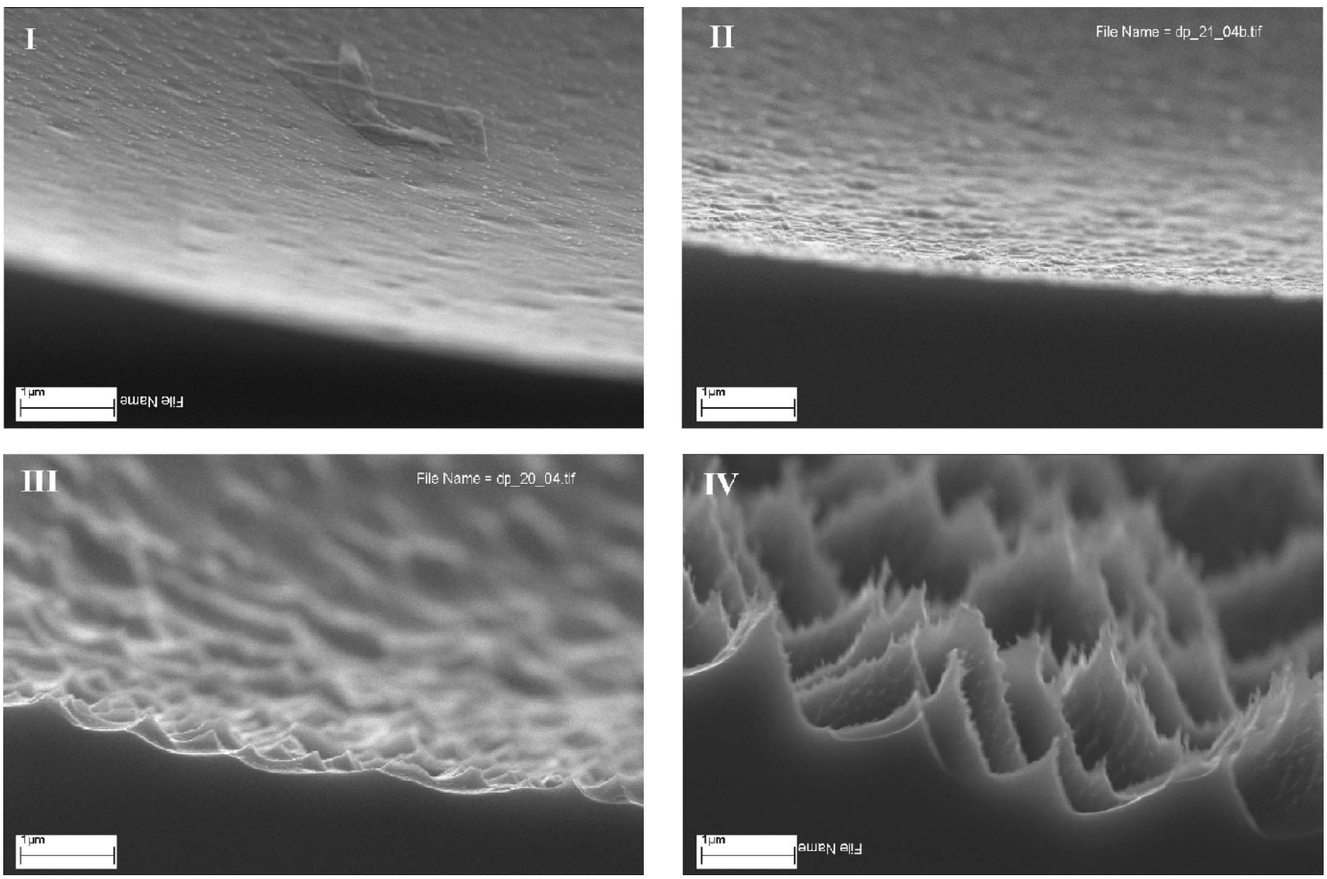

Figure 1. Characteristic surface roughness, as referenced to Table I. Type I is the almost smooth surface, where surface features are difficult to identify. Type II has a very fine-grained and low-amplitude roughness with a flat appearance. Type III has a higher amplitude and a wavelike surface morphology with curved valleys ending in more or less pronounced peaks. Type IV is the high-amplitude roughness characterized by straight sidewalls and curved valleys. The morphology has a clear crystal orientation-dependent nature. The surface of the large roughness peaks has its own smaller scale roughness.

are shown in Fig. 6. After 12 s the surface is still perfectly smooth, but already at a 13 s longer etch duration, the surface is completely covered with needlelike protrusions (the highest is about 0.5 μm tall and ~20 nm wide). The needles are also present at the sidewalls where they point out orthogonally to the surface. At an etch duration of 50 s this roughness seems to have coarsened and grown into larger structures but still of the same type as at 25 s etch duration. Since the direction of the narrow peaks is mostly orthogonal to the surface, they may represent the trajectory of the etching and thereby indicate the etch direction of the surface. At a 150 s etch duration, the geometries have further coarsened and changed character somewhat, now forming more straight-walled roughness peaks with local protrusions. The final etched profile after 300 s etch duration is shown in Fig. 2.

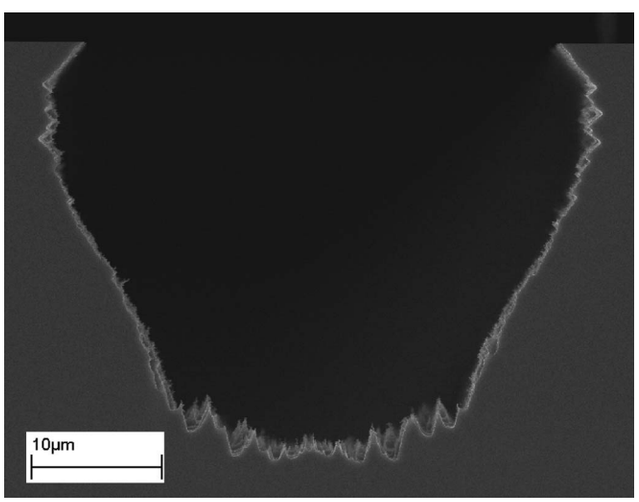

Figure 2. SEM image showing a cross section of the etch profile for a high-roughness etching process, recipe M, here etched for 300 s using a mask width of 7 μm.

The average roughness amplitude grows approximately linearly with the etching depth (corrected for the initial preconditioning etch of 1.1 μm), and the ratio between roughness amplitude and etched depth is 0.085 ± 0.022 at 7 μm mask width. In general, the roughness is assumed to grow linearly with the etch depth, allowing the use of normalized roughness amplitudes. It should be noted that measurement of the roughness amplitudes from SEM images is associated with a relatively high uncertainty.

Crystal orientation dependency.— The roughness of type IV and also to some extent of type III shows a clear crystal orientation dependency. This anisotropy is usually most pronounced for the roughness at the sidewalls shadowed by the mask. Figure 7 shows an example of such faceted sidewall roughness for recipe M; the faceted roughness is also visible in Fig. 2, which shows the etching profile for recipe M. The crystal orientation dependency is also very noticeable when the etch result is observed from above (see Fig. 8),

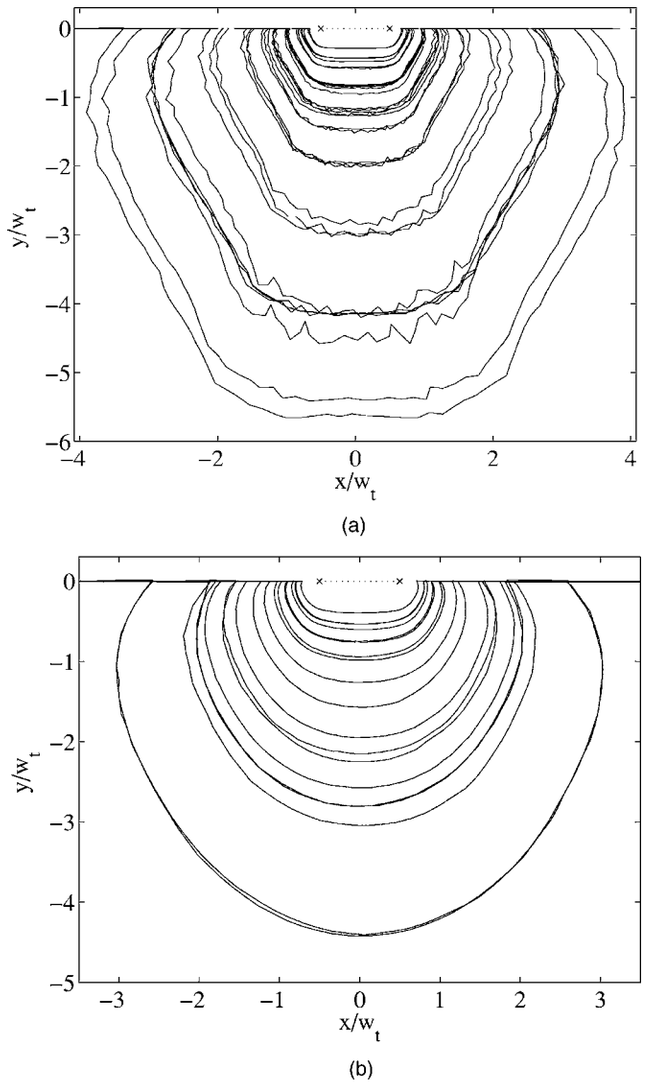

Figure 3. Digitized etched profiles normalized to the mask window width, w_t, for etching processes with an ICP power of 3000 W, window width w_t = 7–180 μm and the pressure p = 70 mTorr (top) or p = 10 mTorr (bottom).

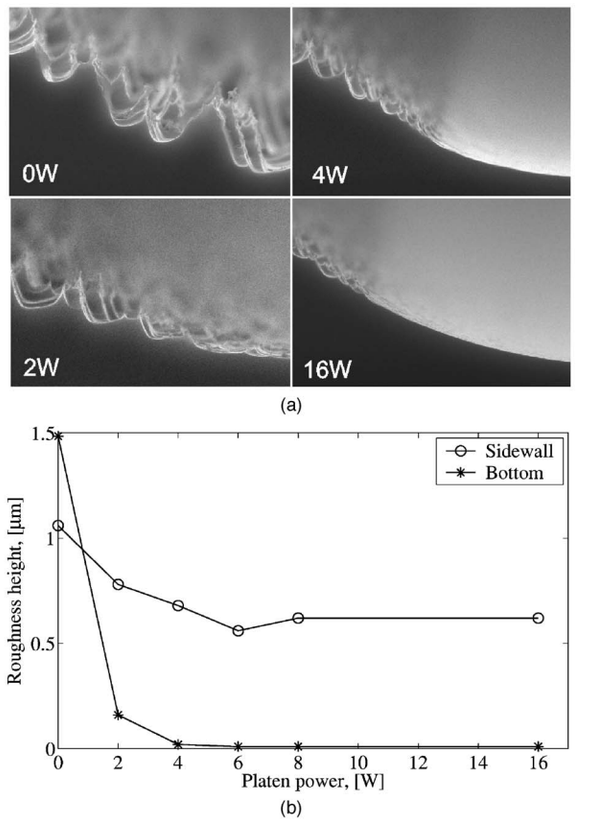

Figure 5. The graph shows the bottom and sidewall roughness as a function of the plating power for an etch based on recipe N/O (180 s). The SEM images show the corresponding bottom roughness morphologies for 0, 2, 4, and 16 W platen power. Note the transition to the areas shadowed under the mask.

where a circular mask aperture was used. The etch facets have a clear relation to the {111} planes of silicon; thus, a fourfold symmetry is observed on a (100) wafer. The etch rates of {110} and {100} planes are less affected, as seen from the two diagonals of the almost circular cavity because they differ by only 2%.

Recipes that cause severe roughness also have characteristic

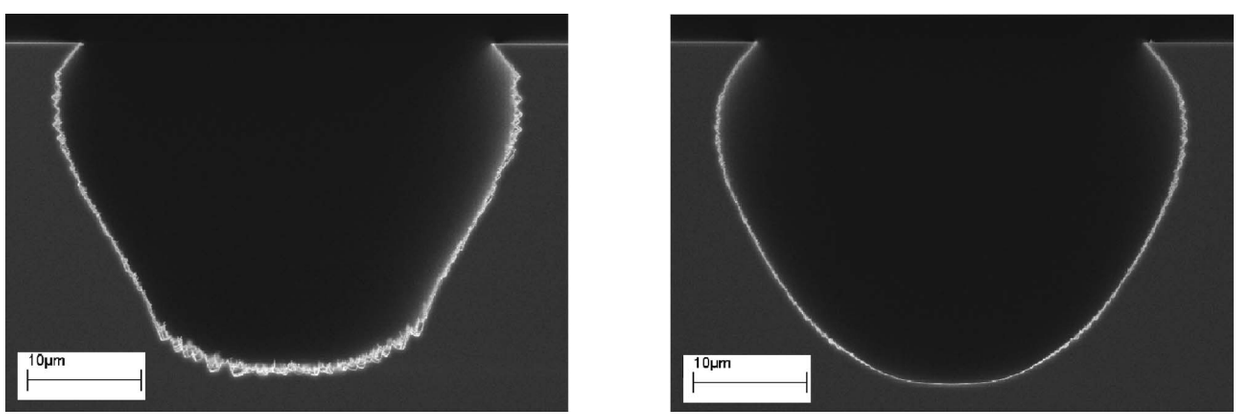

Figure 4. SEM images showing cross sections of the etch profiles from recipes N (left) and O (right). Apart from an applied 16 W platen power for recipe O, the two etches are identical, with an etch duration of 180 s and a mask with of w_t = 7 μm. Due to the narrow mask window the etched depth becomes roughly the same in both processes, since the etching probability P_{etch} becomes independent of P_{stick} when P_{exit} is small.

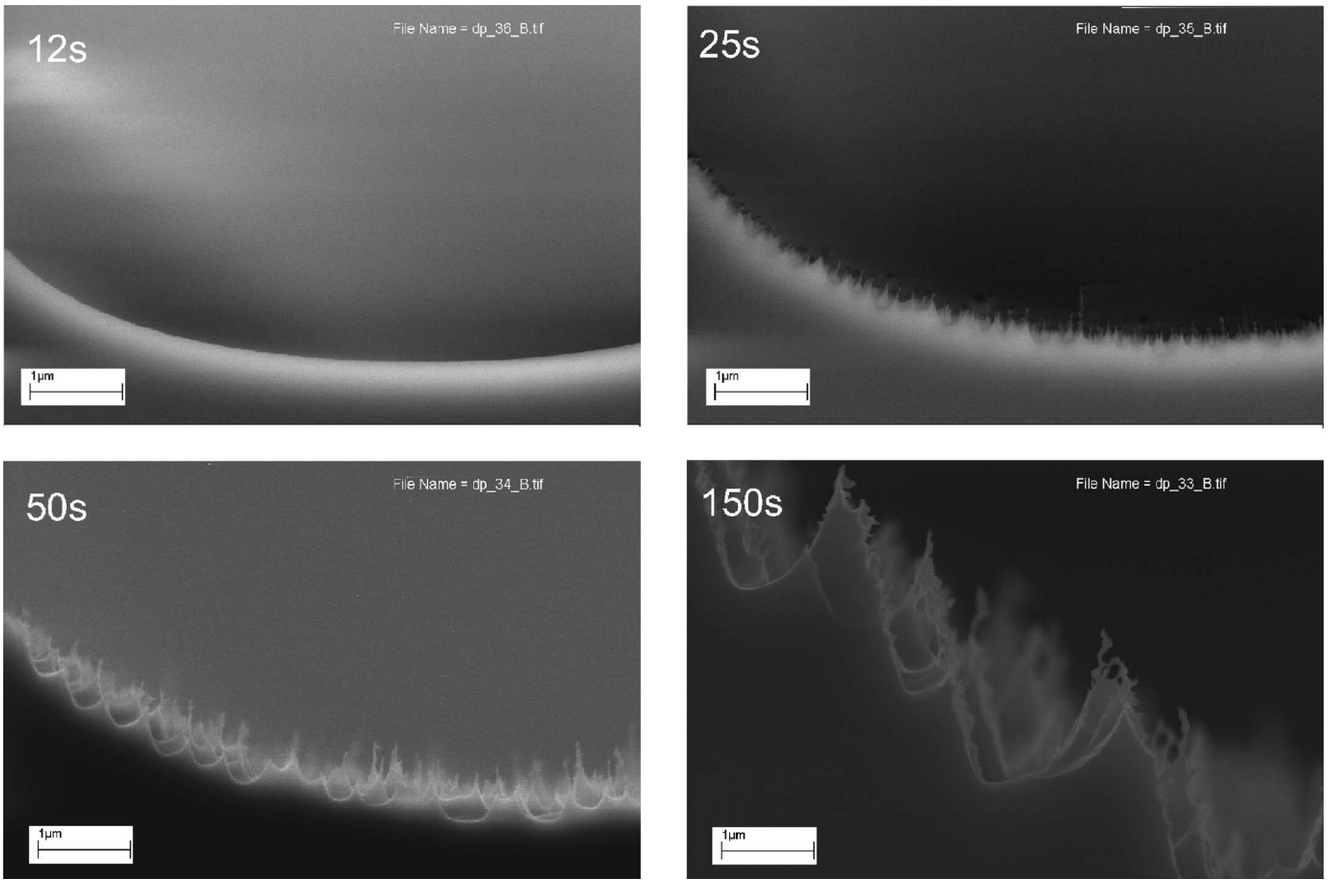

Figure 6. SEM images of the temporal evolution of the roughness for etching processes using recipe M with a mask width of 7 μm at elapsed etch times of 12, 25, 50, and 150 s. Note that the magnification is the same in all images.

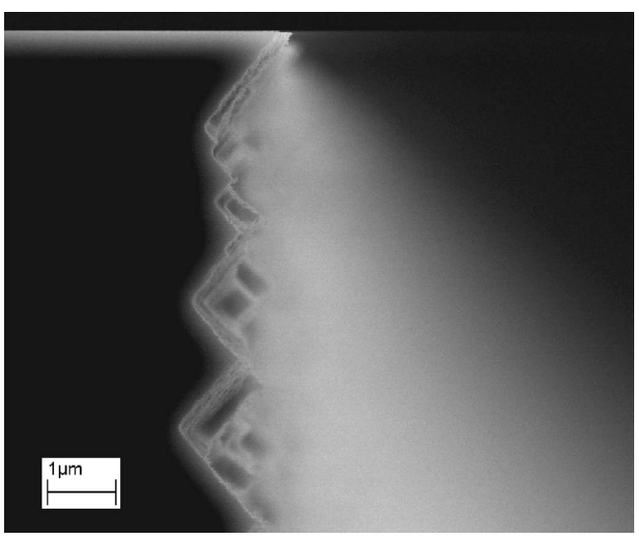

Figure 7. SEM closeup of the sidewall roughness in highly rough etching process, recipe M. The facets of the sidewall roughness have angles in good agreement with the expected angles of {111} planes.

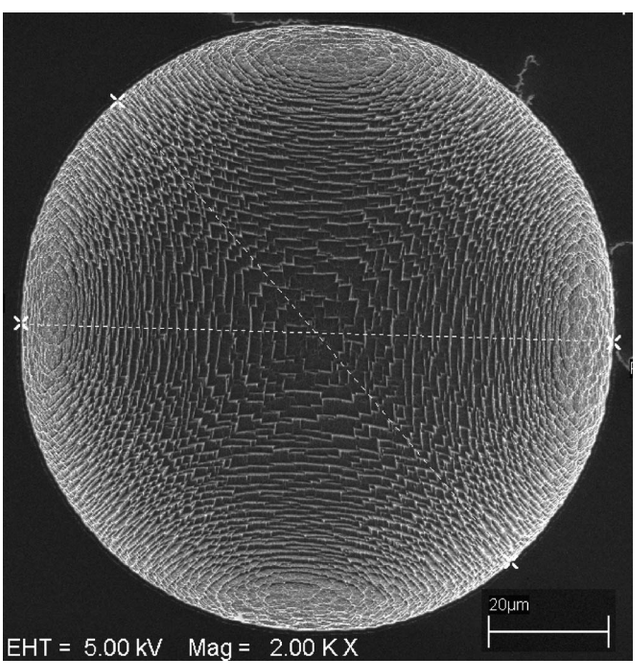

Figure 8. SEM image showing a top view of an etched circular cavity with roughness type IV (etching recipe comparable to recipe I). The crystal-orientation-dependent roughness in the cavity is related to the {111} planes of silicon. The horizontal diameter is 98.7 μm (⟨110⟩ directions), and the 45° diam is 100.8 μm (⟨100⟩ directions); thus, the etch rate differs by only 2% in these crystal directions.

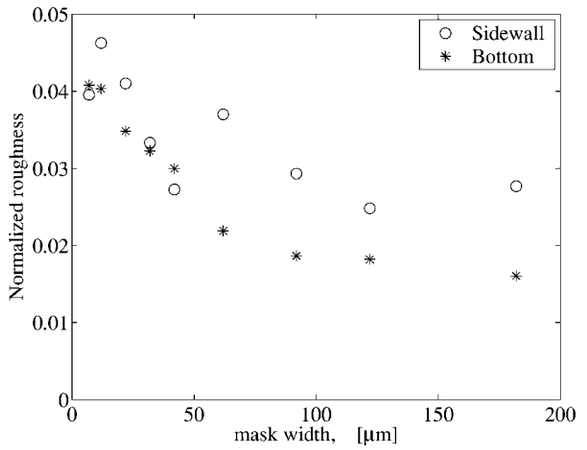

Figure 9. The roughness amplitude normalized to the etched depth as a function of the mask window width for recipe N.

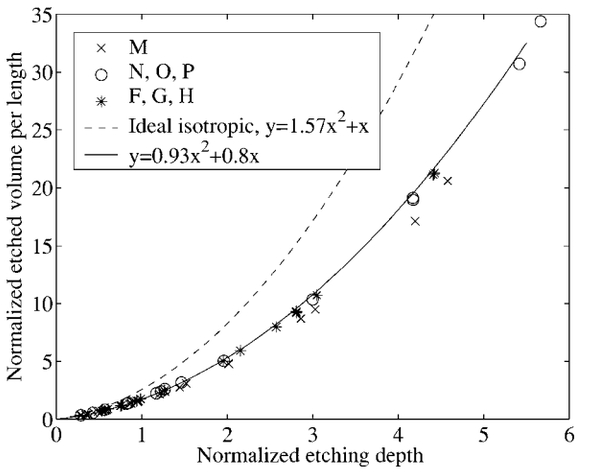

Figure 10. The normalized etched volume per length, $V_{etch}/(Lw_t^2)$, as a function of the normalized etched depth, h_{bot}/w_t.

etched profiles with a straight sidewall region, as seen in Fig. 3 top. The sidewall slopes in Fig. 3 left are fairly constant at ~64°. Even though the angle between {100} and {111} planes of the silicon crystal is 54.7°, this straight wall region could still be related to the {111} planes. The severe roughness seen on the sidewall in Fig. 7 has characteristic angles ~50° to the surface plane. The roughness at the bottom of the trench has a higher characteristic angle, e.g., ~73° for recipe P in Fig. 1 (IV).

The formation of prominent crystal orientation-dependent morphologies seems to be dependent on a low ion energy, which is typical for scattered secondary ions.

The roughness appears to contain fractal geometries, where features are repeated on various length scales. The most prominent crystal-orientation-dependent features are found on the local scale. The etching geometry is very different from usual {111}-plane-sensitive etches such as KOH and cryogenic silicon plasma etching.[11]

Etch profiles and roughness.— The relation between the etching profile and the roughness distribution may help to determine the role of the cavity for the roughness formation and the underlying etching mechanisms. The bottom and sidewall roughness normalized to the corresponding etch depth as a function of the mask aperture is shown in Fig. 9. No changes of the appearance or type of roughness were observed as a function of mask dimensions. The roughness amplitude is seen to decrease as the mask window size, w_t, increases. At large mask windows, however, the normalized roughness seems to reach a constant level of 0.015 and 0.025, respectively. The bottom roughness is consistently smaller than the sidewall roughness, probably due to the primary ion flux to the bottom of the trench compared to the secondary ion flux to the sidewalls. It should be noted that due to the crystallographic dependent nature of the roughness, the height of the local roughness is somehow dependent on the curvature of the profile. Therefore very flat profiles, such as of the bottom of etched trenches with large mask windows, tend to form a lower roughness, compared to more curved profile areas such as the undercut region. This may affect the measurements in Fig. 9.

A general trend for the resulting etched profiles is a remarkably constant anisotropy, h_{bot}/h_{side}, which is found to be $\simeq 1.75 \pm 0.09$ for all the recipes independent of the roughness and platen power. Recipe B, however, was exclusively more anisotropic with an anisotropy of $\simeq 2.2$. Similarly, the normalized etch depth, h_{bot}/w_t, is closely related to the normalized etched volume per unit length, $V_{etch}/(Lw_t^2)$. This relation is shown in Fig. 10 and indicates a one-to-one relation between the normalized etched volume per length and the normalized etched depth, which is almost independent of the roughness. Recipe M, which results in the largest roughness amplitude, deviates slightly from this rule, tending toward a lower etched volume at a given etch depth. For comparison, the expected relation (dashed curve) for a perfectly isotropic etch is also shown in Fig. 10.

Discussion

Etching model.— A simple statistical/geometrical etch model can be developed from conservation of matter arguments as follows. The fluorine radical flux density J_F is incident on the mask window of area A_{mask}. These radicals will be consumed with a total probability P_{etch} consumed in the silicon etching process, where an average of κ radicals are consumed per etched silicon atom. Thus, a molecular flow rate, $J_F A_{mask} P_{etch}/\kappa$, of etched silicon atoms (on average in the form of SiF_κ) out of the mask window results. Since the molecular volume of solid silicon is the ratio of the atomic mass to the mass density, m_{Si}/ρ_{Si}, the etched silicon volume, V_{etch}, in the cavity formed by the mask window is obtained from the differential equation

$$\frac{dV_{etch}}{dt} = \frac{1}{\kappa} J_F A_{mask} P_{etch} \frac{m_{Si}}{\rho_{Si}} \quad [1]$$

This equation can be rearranged in a nondimensional form using a characteristic length scale and a characteristic time scale for the system. The mask window width, w_t, is chosen as the length scale, while the ratio of the length scale to the maximum possible linear etch rate, v_{max}, with the assumed stoichiometry chosen as the time scale, w_t/v_{max}; here $v_{max} = \frac{1}{\kappa} J_F m_{Si}/\rho_{Si}$. The dimensionless etched volume, $\tilde{V}_{etch}$, becomes $\tilde{V}_{etch} = V_{etch}/(A_{mask} w_t)$. For a mask window realizing a trench of length L, the dimensionless etched volume thus is $\tilde{V}_{etch} = V_{etch}/(Lw_t^2)$, while the dimensionless time becomes $\tilde{t} = t v_{max}/w_t$. The result is the scaled differential equation

$$\frac{d\tilde{V}_{etch}}{d\tilde{t}} = P_{etch} \quad [2]$$

The probability, P_{etch}, that a fluorine radical is consumed in the etching process is dependent on both the geometry of the cavity and the local sticking coefficient, P_{stick}, for the radicals. If the radical does not stick at the silicon surface, it is assumed to be reflected in a random direction. The geometrical probability for the radical to escape out of the mask window after such a reflection, P_{exit}, is shown in Fig. 11 as a function of the normalized etched volume. Since the mean-free path of the radicals is long compared to the dimensions of the etched cavities, a collisionless line of sight model is appropriate; thus, P_{exit} is obtained directly from the etched pro-

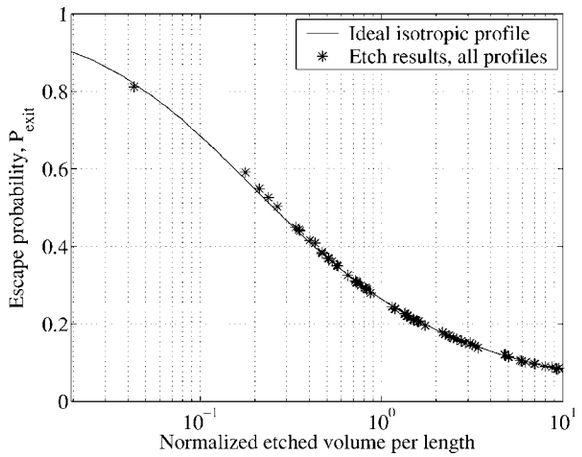

Figure 11. The escape probability, P_{exit}, of a radical through the mask window as a function of the normalized etched volume per length, $V_{etch}/(Lw_t^2)$.

files, by taking the average of the point of view angle of the mask opening, θ_{exit}, for each point on the profiles. Then $P_{exit} = \langle\theta_{exit}\rangle/\pi$. The experimental escape probability is very close to the expected values for a perfectly isotropic etch, as indicated by the full curve in Fig. 11. It follows that the escape probability is quite insensitive to the actual shape of the profile and can be well approximated by a function of the normalized etched volume only. By combining P_{stick} with P_{exit}, the total probability, P_{etch}, for the radical to stick (etch) inside the cavity can be found to be

$$P_{etch} = \frac{P_{stick}}{P_{exit} + P_{stick} - P_{exit}P_{stick}} \quad [3]$$

which is a function of the normalized etched volume.

Figure 12 shows the model fitted to experimental etch data from recipes G, M, and N, and Table II shows the corresponding extracted model parameters from the fit to profiles of recipes G, M, N, and O. In general, it was possible to obtain very good agreement between the experimental profiles and the model, especially in the range of low normalized etched volumes, as seen in Fig. 12.

For recipe N the resulting sticking coefficient was $P_{stick} = 0.26$, while for recipe G it was $P_{stick} = 0.37$.

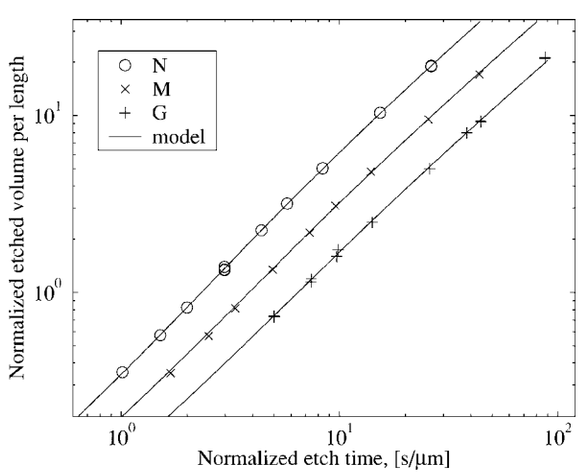

Figure 12. Experimental profile data and results from the etching model plotted against the normalized etching time, t_{etch}/w_t.

Table II. Extracted etch model parameters, sticking coefficient, P_{stick}, and radical flux density, J_F. See also Fig. 12.

Recipe ID	Etch time (s)	P_{stick}	Flux J_F (cm^{-2} s^{-1})
G	300	0.37	5.39×10^{18}
M	50	0.39	1.02×10^{19}
M	150	0.35	1.02×10^{19}
M	300	0.32	1.00×10^{19}
N	180	0.26	1.92×10^{19}
O	180	0.32	1.90×10^{19}

Thus, the model indicates that P_{stick} is lower for the rough than for the smooth etching processes, which may indicate the presence of a surface passivation layer for the rough etching processes.

Recipe O has increased ion energy due to the applied platen power, but otherwise the same radical and ion fluxes as for recipe N are expected. The best fit from the model to recipe O (not shown) indicates a slight increase of the sticking coefficient, $P_{stick} = 0.32$, compared to 0.26 in recipe N but essentially the same radical flux.

The model was fitted to the profiles from the time evolution experiments, where recipe M was used, and here a gradually decreasing sticking coefficient was expected due to the effect of passivation material deposition. The model fits data well using a radical flux of $J_F \simeq 1.0 \times 10^{19}$ cm^{-2} s^{-1} and a sticking coefficient of 0.39 up to 50 s etch duration, whereafter the sticking coefficient declines to 0.35 at 150 s and 0.32 at 300 s, as seen in Table II.

Note, the model does not take into account the increase in surface area due to roughness and possible local variations; thus, the real sticking coefficients are lower than the extracted ones, which thus should be considered effective sticking coefficients.

The radical flux values extracted from the model are of the right order of magnitude but are slightly higher than expected from mass conservation models of the system, probably due to a different net stoichiometry of the reaction product, e.g., $\kappa < 4$. Most probably κ, is in the range between 2 and 4, which is consistent with the extracted radical flux values, as they are really $\frac{4}{\kappa}J_F$.

Etch behavior.— The results from the model suggest that all the etch recipes, no matter whether the etch result is smooth or rough, can be described by a highly chemical and radical-dependent etching mechanism. Numerical simulations of purely radical-dependent etching processes with P_{stick} between 0.1 and 0.5 by Marcos et al.[14] show etching profiles comparable to the smooth etched profiles in this work. The rough etching profiles are much more faceted, but the overall anisotropy of the rough profiles is the same as for the smooth profiles.

For a radical-dependent etch, the ion flux to all surfaces is sufficient not to limit the etch rate. The ion flux at the sidewalls, which are shadowed from the primary ion flux by the mask, thus consists of secondary ions reflected from the bottom of the trench. Ion trajectories affected by electrostatic charging of the mask have been discussed in the literature and are not believed to contribute significantly to ion flux in the areas shadowed by the mask.[15]

Much evidence indicates that the observed roughness is caused by a passivation layer that gradually builds up during the etch process. However, this layer does not reduce the overall etch rate significantly. Increasing the ion energy can inhibit formation of the passivation layer and thus reduce the roughness. The exact threshold energy is not known, since we do not have access to bias voltage measurement on the etching equipment used.

Surprisingly, increasing the ion energy does not result in higher anisotropy of the etching process, just a change to profiles comparable to the smooth etching profiles. The sticking probability obtained from the model shows a slight reduction from $P_{stick} \sim 0.4$ for a smooth etching process to $P_{stick} \sim 0.3$ for a highly rough etching process. The passivation layer thus only seems to have a minor passivating effect on the surface. This is illustrated in Fig. 7, where

the rough sidewall surface, which is assumed to be covered with a roughness-causing passivation layer, still has a high etch rate, ~11 μm/min, horizontally. Such high etch rates of passivated surfaces may promote a very high mobility and redistribution of the passivation material by diffusive transport, but it may also suggest that the passivation layer could be very thin, maybe only a fraction of a monolayer.

Roughness formation.— The roughness of type III and IV observed in this study is not directly comparable to that found in other roughness studies,[4-6,8] mainly due to the well-known presence of a roughness-causing passivation material on the etched surfaces in this study. Correspondingly, the resulting roughness amplitude is much higher, typically in the micrometer range, compared to 10–20 nm as typically reported. Type I and II roughness, however, may be comparable to the roughnesses reported by Ref. 4-6 and 8.

We suggest that the primary parameters controlling the roughness evolution are the local passivation material coverage and the local etch rate of the surface. The local etch rate here plays an important role for the mobility and redistribution of the passivation material. We propose the following formation mechanisms for the observed roughness.

Type II, granular roughness.— The lowest amplitude roughness shows a granular appearance, which may result from a low passivation material coverage where microclusters or microislands are favored. Intrinsic instabilities of the etch front as discussed in Ref. 5 and 8 may also play a role in this low-amplitude roughness.

Type III, wavy roughness.— The wavy morphology may be explained by an increased passivation material coverage combined with a considerable redistribution during the etching process. Looking at the roughness morphology, it appears that the etch process is nearly isotropic in the valleys. This results in expanding surfaces and thereby a reduction of the surface passivation material coverage. The opposite happens at the peaks, where the etch process reduces the surface area and thus increases the passivation material coverage. The net result is a transport of passivation material toward the roughness peaks, causing the wavy morphology. In certain cases this may result in completely passivated narrow spikes. With this mechanism, the spike direction is not determined by the ion or radical directionality but by the local etch direction. This mechanism also accounts for the roughness spikes pointing out from the surface as observed at the sidewalls.

Type IV, high-amplitude, crystal-orientation-dependent roughness.— At an even higher passivation material coverage, the roughness grows in amplitude and shows a clear crystal-orientation-dependent morphology. Facets at angles close to the angles of {111} planes appear on the rough surface. The precise mechanism is not understood, but we suggest that the interface energy of the silicon–passivation material system could be anisotropic, such that the desorption energy of the passivation material is higher on a {111} surface. As a result, passivation material would accumulate on {111} surfaces revealed during the etching process and cause the facets to appear.

Passivation material.— We observe a clear correlation between the roughness and the process parameters such as pressure and flow rate, while the effect from the internal geometrical etching conditions inside the cavity is less significant. A very deep etch through small mask windows (low P_{exit}) only shows an increased roughness amplitude (see Fig. 9), while the fundamental roughness morphology seems to be unaffected. This is important as geometry has a significant effect on the number of internal hits from internal reflections of not only radicals and ions, but also from reaction products and redistributed surface contamination.

The external plasma conditions have a much more direct effect. The photoresist mask, most likely through a general contamination of the plasma with photoresist-related material, induces the deposition of passivation material. Whether this passivation material consists of molecules from the resist mask or various derived reaction products is not known. The dramatic increase of the roughness when the pressure is raised may relate to parameters such as the photoresist mask erosion rate, the ion energy, and the residence time of the system. Further studies are needed in order to clarify these mechanisms. The increased roughness amplitude seen for narrow mask windows (see Fig. 9) might be due to additional passivation material originating from the mask edge, as such a contribution would increase in relative magnitude when the window size is reduced.

Conclusions

We have studied the roughness and the etch profiles resulting from photoresist-masked, pure SF_6 plasma silicon etch in an ICP etch tool at varying process conditions. Processes at a pressure of 10 mTorr and no platen power show low roughness at the bottom of the etched trenches and a slightly higher roughness at the sidewalls. At higher pressure (40–70 mTorr) the entire etched surface shows much higher roughness amplitudes, with increasing amplitudes for etching processes at low flow rates. The roughness morphology at these process conditions shows a clear crystallographic anisotropy, where {111} planes are revealed. The roughness is probably caused by a buildup of surface passivation material originating from contamination from the photoresist mask. Applying a platen power of 4 W or above reduces the bottom roughness dramatically. This increased ion energy also has a significant roughness-reducing effect on the sidewalls. We propose an etching mechanism where high-aspect-ratio roughness such as nanospikes is formed from a redistribution of the contamination on the surface during the etching process and is thus unrelated to the directionality of ions or radical flux. The etching mechanism for both the rough and smooth etching processes was shown to be highly radical-dependent. The sticking coefficient for the smooth and rough etch processes was estimated to 0.4 and 0.3, respectively, which indicates only a minor etch rate reduction from the passivation material causing the roughness.

Acknowledgments

The Center for Individual Nanoparticle Functionality (CINF) is sponsored by The Danish National Research Foundation.

The Technical University of Denmark assisted in meeting the publication costs of this article.

References

1. T. Yi and C. Kim, *Meas. Sci. Technol.*, **10**, 706 (1999).
2. M. Zeman, J. W. van Swaaij, and R. Metselaar, *J. Appl. Phys.*, **88**, 6436 (2000).
3. K. Lau, J. Bico, K. Teo, M. Chhowalla, G. Amaratunga, W. Milne, G. McKinley, and K. Gleason, *Nano Lett.*, **3**, 1701 (2003).
4. R. Petri, P. Brault, O. Vatel, D. Henry, E. Andre, P. Dumas, and F. Salvan, *J. Appl. Phys.*, **75**, 7498 (1994).
5. J. T. Drotar, T.-M. Zhao, Y.-P. abd Lu, and G.-C. Wang, *Phys. Rev. B*, **61**, 3012 (2000).
6. P. Brault, P. Dumas, and F. Salvan, *J. Phys. Condens. Matter*, **10**, 27 (1998).
7. N. O. V. Plank, M. A. Blauw, E. W. J. M. van der Drift, and R. Cheung, *J. Phys. D*, **36**, 482 (2003).
8. E. Gogolides, C. Boukouras, G. Kokkoris, O. Brani, A. Tserepi, and V. Costantoudis, *Microelectron. Eng.*, **73–74**, 312 (2004).
9. H. Jansen, R. Meint de Boer, R. Legtenberg, and M. Elwenspoek, *J. Micromech. Microeng.*, **5**, 115 (1995).
10. R. Dussart, M. Boufnichel, G. Marcos, P. Lefaucheux, A. Basillais, R. Benoit, T. Tillocher, X. Mellhaoui, H. Estrade-Szwarckopf, and P. Ranson, *J. Micromech. Microeng.*, **14**, 190 (2004).
11. M. Blauw, T. Zijlstra, R. Bakker, and E. van der Drift, *J. Vac. Sci. Technol. B*, **18**, 3453 (2000).
12. C. Linder, T. Tschan, and N. de Rooij, in *Digest of Technical Papers, International Conference on Solid-State Sensors and Actuators, TRANSDUCERS'91*, pp. 524–527 (1991).
13. K. P. Larsen, J. T. Ravnkilde, and O. Hansen, *J. Micromech. Microeng.*, **15**, 873 (2005).
14. G. Marcos, A. Rhallabi, and P. Ranson, *J. Vac. Sci. Technol. A*, **21**, 87 (2003).
15. M. Boufnichel, P. Lefaucheux, S. Aachboun, R. Dussart, and P. Ranson, *Microelectron. Eng.*, **77**, 327 (2005).